Catal Lett (2009) 127:339–347
DOI 10.1007/s10562-008-9686-z

Macroporous Monolithic Pt/γ-Al_2O_3 and K–Pt/γ-Al_2O_3 Catalysts Used for Preferential Oxidation of CO

Yuan Zhang · Cun Yu Zhao · Hao Liang · Yuan Liu

Received: 9 July 2008 / Accepted: 17 September 2008 / Published online: 10 October 2008

Abstract Macro-porous monolithic γ-Al_2O_3 was prepared by using macro-porous polystyrene monolith foam as the template and alumina sol as the precursor. Platinum and potassium were loaded on the support by impregnation method. TG, XRD, N_2 adsorption–desorption, SEM, TEM, and TPR techniques were used for catalysts characterization, and the catalytic performance of macro-porous monolithic Pt/γ-Al_2O_3 and K–Pt/γ-Al_2O_3 catalysts were tested in hydrogen-rich stream for CO preferential oxidation (CO-PROX). SEM images show that the macropores in the macro-porous monolithic γ-Al_2O_3 are interconnected with the pore size in the range of 10 to 50 μm, and the monoliths possess hierarchical macro-meso(micro)-porous structure. The macro-porous monolithic catalysts, although they are less active intrinsically than the particle ones, exhibit higher CO conversion and higher O_2 to CO oxidation selectivity than particle catalysts at high reaction temperatures, which is proposed to be owing to its hierarchical macro-meso(micro) -porous structure. Adding potassium lead to marked improvement of the catalytic performance, owing to intrinsic activity and platinum dispersion increase resulted from K-doping. CO in hydrogen-rich gases can be removed to 10 ppm over monolithic K–Pt/γ-Al_2O_3 by CO-PROX.

Y. Zhang · C. Y. Zhao · H. Liang · Y. Liu (✉)
Tianjin Key Laboratory of Applied Catalysis Science and Engineering, Department of Catalysis Science and Technology, School of Chemical Engineering and Technology, Tianjin University, Tianjin 300072, China
e-mail: yuanliu@tju.edu.cn

Y. Zhang
e-mail: llwinwill@163.com

Keywords Monolith · Macropore · Preferential oxidation · Platinum · Potassium · Alumina

1 Introduction

1.1 CO Preferential Oxidation (CO-PROX)

The polymer exchange membrane fuel cell (PEMFC) has come to be regarded as one of the most promising candidates for utilizing hydrogen to produce heat and electricity, especially for electric vehicles, residential co-generation systems and portable power supplies for small devices [1, 2]. Hydrogen-rich gas production for fuel cells is mainly by using reforming or partial oxidation of hydrocarbons followed by water gas shift reaction. The resultant gas mixtures contain about 1 vol.% CO. The concentration of CO must be reduced to lower than 10 ppm, because the Pt anode in PEMFC is sensitive to CO [3]. CO-PROX is known to be the most promising method for reducing the carbon monoxide under 10 ppm [1–3].

The main reactions in CO-PROX process include:

$$\text{Desired reaction: } CO + \frac{1}{2}O_2 \rightarrow CO_2 \quad (1)$$

$$\text{Undesired reactions: } H_2 + \frac{1}{2}O_2 \rightarrow H_2O \quad (2)$$

$$CO + 3H_2 \rightarrow CH_4 + H_2O \quad (3)$$

Reaction (2) and (3) consume hydrogen, reducing the selectivity of desired reaction (1), so they ought to be avoided.

The catalysts studied for CO-PROX include: (1) noble metal catalysts, such as Pt, Rh and Pt modified by transition metal or alkali metal [4–13]; (2) Au-based catalysts

[13, 14]; and (3) non-noble metal oxide catalysts [14–17]. Among all of them, platinum-based catalysts are considered to be the most potential candidate for application, because of their highly stable performance and excellent resistance to CO_2 and H_2O [18].

So far, although extensive research has been done, it still remains a hard work for removing CO in hydrogen-rich gases to under 10 ppm [3, 16, 19, 20]. Up to now, the investigation and exploration on CO-PROX catalysts have been concentrated on its structure, reaction mechanism, catalytic performance, preparation method and new catalytic materials, in order to design or to find catalysts with high intrinsic activity and high selectivity.

To overcome this issue, adjusting our thinking to another direction may be helpful. It is known that CO oxidation, reaction (1), is very rapid, and as the CO conversion is close to 100%, the reaction should be transfer limited. Chin et al. [7, 8] studied Pt–Fe/Al_2O_3 catalysts supported on metal foam (pore size in millimeter scale), and found that a significant mass transfer resistance between the bulk gas and the catalyst surface existed, which decreased the CO conversion and selectivity of the PROX reaction. Over monolithic catalysts, the external resistance to mass transfer is a main reason to the incomplete conversion of CO. Srinivas et al. [9] investigated the Pt/Al_2O_3 catalyst coated on a silicon micro-channel reactor for the PROX reaction (the channel width is 200 μm × 400 μm), and proposed that this wall-coated catalyst didn't introduce any loss of performance efficiency due to external diffusive limitations, while the internal transport resistance might be existent. In addition, in the hydrogen-rich gas system, the content of H_2 is much higher than CO, and H_2 is easier to diffuse than CO, so reaction (2) should not be a transfer limited reaction. Thus, it is proposed that to improve the CO conversion and selectivity for CO-PROX, the transfer of CO should be a key factor. So the porosity design of catalysts, which is a key factor for transfer, is crucial.

1.2 Macro-Porous Monolith Materials

Macro-porous materials with interconnected macro-porous structure are widely studied for application in optical and catalytic materials, filtration and separation, reactors for large molecular reaction, and so on [21]. Recently, macro-porous materials used as catalysts or catalyst supports for large molecular reactions have been attracting much attention. Chen et al. [22] prepared macro-porous FCC catalysts and HDS catalysts using polystyrene spheres as template for heavy oil processing, and found that the macro-porous catalysts were much more active than the catalysts prepared without templates, owing to the macro-porous catalysts were beneficial to mass transfer. Tan et al. [23] found that macro-meso-micro-porous MY/kaolin composite catalysts exhibited excellent activity in heavy crude oil cracking. Somma et al. [24] prepared niobia-silica xeogel, aerogel and MCM type materials used for epoxidation of cyclohexene with hydrogen peroxide, and found that meso-macro-porous aerogel was a stable and recyclable catalyst.

As mentioned above, for CO-PROX process, the desired reaction (1) is diffusive limited, while the side reaction (2) is not diffusive limited. So, if weakening or eliminating the diffusive resistance by optimizing the pore structure of the catalysts, the conversion of reaction (1) will be enhanced without changing the conversion of the side reactions. As a result, optimizing the pore structure of the catalysts could improve the CO purification effect without sacrificing selectivity.

Applying macro-porous materials to small molecular reaction, such as CO-PROX, has been rarely reported so far. However, based on the above analysis, designing of pore structure should be of great significance for CO-PROX. Hence, in this work, macro-meso(micro)-porous monolithic Pt/γ-Al_2O_3 and K–Pt/γ-Al_2O_3 catalysts were prepared and applied to CO-PROX. It is shown that the macro-meso(micro)-porous monoliths are efficient for removing CO from hydrogen-rich gases.

2 Experimental

2.1 Preparation of Macro-Porous Monolithic Pt/γ-Al_2O_3 and K–Pt/γ-Al_2O_3 Catalysts

2.1.1 Preparation of Monolithic Polystyrene Foam Template

The polystyrene foams were obtained by polymerization of styrene in highly concentrated water-in-oil (W/O) emulsions. Both of the monomer styrene (Tianjin Reagent Co., China) and the crosslink agent divinylbenzene (DVB, Alfa Aesar, UK) were washed with 0.2 mol L^{-1} NaOH and then with deionized water. Styrene (2.0 g), DVB (0.5 g), AIBN (20 mg, Tianjin Reagent Co., China) and Span 80 (90 mg, Tianjin Reagent Co., China) were introduced into a flask to form a homogeneous phase. Then water was added dropwisely into the homogeneous phase with a syringe at room temperature under stirring, until the volume fraction of the water reached 0.82. Thus the highly concentrated water-in-oil (W/O) emulsion was generated. The emulsion was put into sealed glass molds with the temperature holding at 60 °C for 24 h, during which polymerization of styrene was proceeding. The wet polystyrene monoliths were removed from the molds by carefully breaking the glass containers, then washed with deionized water and ethanol

to remove surfactant species, and dried at 60 °C for 24 h, obtaining polystyrene monolithic templates.

2.1.2 Preparation of Macro-Porous Alumina Monolith

Macro-porous alumina monoliths were prepared by imbibing macro-porous polystyrene foams with the alumina sols. The sols were prepared as follows: 4 g pseudo-boehmite was put into 60 mL deionized water under stirring. After 1 h aging, 1 M HNO_3 was dropped into the system with a ratio of $n(Al^{3+}):n(H^+) = 1:0.03$. A translucent alumina sol was obtained by aging it for 12 h under stirring at room temperature. The alumina sol was imbibed into the polystyrene template pores under modest vacuum, and the thus coated templates were dried at 60 °C for 12 h. The coating and drying procedures were repeated for several times. The coated templates were calcined in air at 600 °C for 4 h to obtain macro-porous alumina monoliths. The heating rate was 1 °C min^{-1}.

2.1.3 Preparation of Macro-Porous Monolithic Pt/γ-Al_2O_3 and K–Pt/γ-Al_2O_3 Catalysts

Macro-porous monolithic Pt/γ-Al_2O_3 catalysts (denoted as M-Pt/γ-Al_2O_3) were prepared by impregnating the alumina monoliths with an aqueous solution of H_2PtCl_6 for 12 h. After the impregnation, the samples were dried under 200 W microwave for 20 min, and then calcined in air at 500 °C for 2 h. The loading amount of platinum was 1 wt.%. Macro-porous monolithic K–Pt/γ-Al_2O_3 catalysts (denoted as M–K–Pt/γ-Al_2O_3) were prepared by step-impregnation. The M–Pt/γ-Al_2O_3 catalyst precursors, which are the samples after microwave drying and before calcination, were impregnated with an aqueous solution of K_2CO_3, then they were dried under 200 W microwave for 20 min and calcined at 500 °C for 2 h. The loaded potassium is in molar ratio of K/Pt = 10 [4].

For comparison, particle catalysts of 1 wt.% Pt/γ-Al_2O_3 (denoted as P–Pt/γ-Al_2O_3) were prepared by incipient impregnation. Prior to the impregnation, the alumina support (Shanxi Chemicals Institute, China) was calcined at 600 °C for 2 h in air. The impregnated samples were dried at 110 °C for 12 h, and calcined at 500 °C for 2 h.

For comparison too, M–Pt/γ-Al_2O_3 catalyst was crushed and then tabletted by a tabletting machine with a pressure of 11 MPa to destroy the macro-porous structure. The resulted samples are named as crushed M–Pt/γ-Al_2O_3.

2.2 Characterization

Thermo gravimetric analysis was carried out on a Perkin–Elmer Pyris TG instrument at a dry-air atmosphere with a heating rate of 10 °C min^{-1}.

Powder X-ray diffraction (XRD) patterns of the samples were recorded on Rigaku D/max 2500v/pc X-ray diffractometer in order to identify the different phases present in the samples and to determine their crystalloid. Copper Kα radiation ($\lambda = 0.15406$ nm) was used with a power setting of 40 kV and 100 mA (Scan rate = 5 min^{-1}).

Photographs of the monoliths were taken by using an Olympus μ7000 digital camera.

Scanning electron microscopy (SEM) tests were performed on a Philips XL-30ESEM microscope with Au-sputtered specimen operated at 15 keV to observe the macro-porous structures of the samples.

Nitrogen adsorption and desorption isotherms were determined on a Micromeritics apparatus of model ASAP-2020 system at −196 °C. The specific surface areas were calculated by the BET method and the pore size distributions were calculated from the adsorption branch of the isotherm by BJH model.

Transmission electron microscopy (TEM) pictures were obtained on a Technai G^2 F20 microscope operated at 200 kV. Samples were pre-reduced at 500 °C in 5 vol.% H_2–N_2 gas mixtures for 1 h, then finely grounded in a mortar to fine particles and dispersed ultrasonically in ethanol. The well dispersed samples were deposited on a Cu grid covered by a holey carbon film for measurements.

Temperature programmed reduction (TPR) experiments were carried out in a quartz reactor with a reduction gas mixtures of 5 vol.% H_2–Ar and at a heating rate of 10 °C min^{-1}. 100 mg samples were used and were pretreated in He at 300 °C for 1 h in each run. TCD was used as detector.

2.3 Catalytic Performance Test

Catalytic performance tests were carried out in a fixed tubular reactor operated at atmospheric pressure. In each run, a piece of monolith was put into a high temperature resistant silicone tube, and the silicone tube was connected with two quartz tube (400 mm length, 6 mm i.d.) at its both sides. The reaction temperature was monitored by a K-type thermocouple placed in the monolithic catalysts and controlled by a temperature controller. The reaction mixtures consisted of 1 vol.% CO, 1 vol.% O_2, and 50 vol.% H_2 in N_2. The mass space velocity was 80,000 mL g_{cat}^{-1} h^{-1} and the corresponding volume space velocity was 20,000 h^{-1}. The reactant and product mixtures were analyzed with a SP-3420 gas chromatograph (GC) equipped with a thermal conductivity detector (TCD) and a column packed with 5A molecular sieve. A methane convertor was used to magnify the CO signals. A hydrogen flame ionization detector (FID) was equipped to detect the CH_4 and CO signals. The detection limit for CO is 5 ppm. CO and O_2 conversion, the selectivity of O_2 to CO oxidation and yield of CH_4 were calculated by the following formulae:

$$\text{Conversion of CO } (\%): X_{CO} = \frac{[CO]_{in} - [CO]_{out}}{[CO]_{in}} \times 100 \quad (5)$$

$$\text{Conversion of } O_2(\%): X_{O_2} = \frac{[O_2]_{in} - [O_2]_{out}}{[O_2]_{in}} \times 100 \quad (6)$$

$$\text{Selectivity of } O_2 \text{ to CO } (\%): S_{O_2} = \frac{[CO]_{in} - [CO]_{out} - [CH_4]_{out}}{2 \times ([O_2]_{in} - [O_2]_{out})} \times 100 \quad (7)$$

$$\text{Yield of } CH_4(\%): Y_{CH_4} = \frac{[CH_4]_{out}}{[CO]_{in}} \times 100 \quad (8)$$

3 Results and Discussions

3.1 TG and XRD

Figure 1 is the TG curve of the Al_2O_3/PS composite, i.e., the polystyrene foam filled with alumina sol after drying. From room temperature to 800 °C, there are four obvious weight loss stages. (1) Before 100 °C, a weight loss of 8% is caused by the evaporation of surface water. (2) From 100 °C to 300 °C, a weight loss of 8% is due to the evaporation of structural water. (3) The large weight loss of 50% between 300 °C and 370 °C is attributed to the combustion of the polystyrene template. (4) In the temperature range of 370 °C to 550 °C, a weight loss of 22% is owing to the transformation from γ-AlOOH to γ-Al_2O_3. As temperature is higher than 550 °C, no weight loss could be detected. The total weight loss is about 88%.

Figure 2 presents the XRD patterns of the alumina supports and catalysts. It can be clearly seen that all samples obtained the cubic γ-Al_2O_3 phase (JCPDS No. 10-0425) [25]. The monolithic samples show sharper diffraction peaks than the particle ones, which indicates that the crystallite size of the monolithic samples is slightly larger.

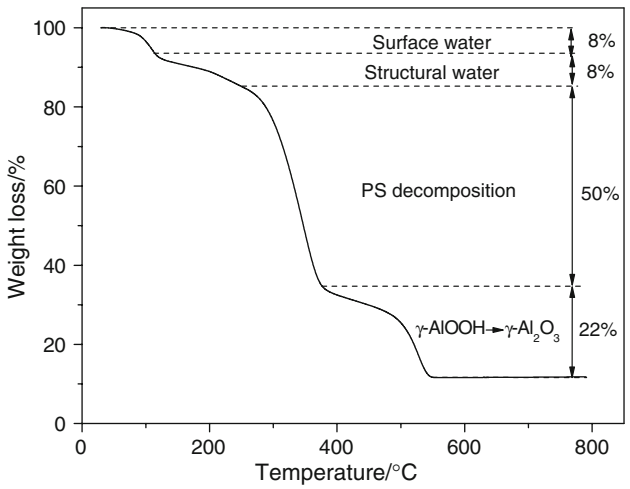

Fig. 1 TG curve of the Al_2O_3/PS composite

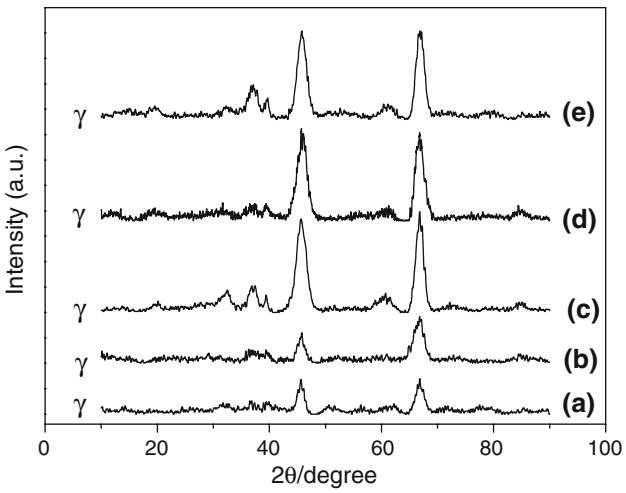

Fig. 2 XRD patterns of **a** P-γ-Al_2O_3, **b** P–Pt/γ-Al_2O_3, **c** M-γ-Al_2O_3, **d** M–Pt/γ-Al_2O_3 and **e** M–K–Pt/γ-Al_2O_3

3.2 Photographs and SEM Images

Examples of the bulk morphology of the PS foams and resultant supports and catalysts are shown in Fig. 3. Figure 3a shows an optical photograph of the bulk-molded PS monolith with a cylindrical shape, while Fig. 3b shows the corresponding bulk macro-porous alumina monolith prepared from it. During calcination to move the organic templates, shrinkage of the monoliths occurs. Comparing to the original PS foams, the bulk shapes of alumina monoliths appear to replicate the templates with shrinkage of approximately 30% reduction in bulk monolith dimensions. The

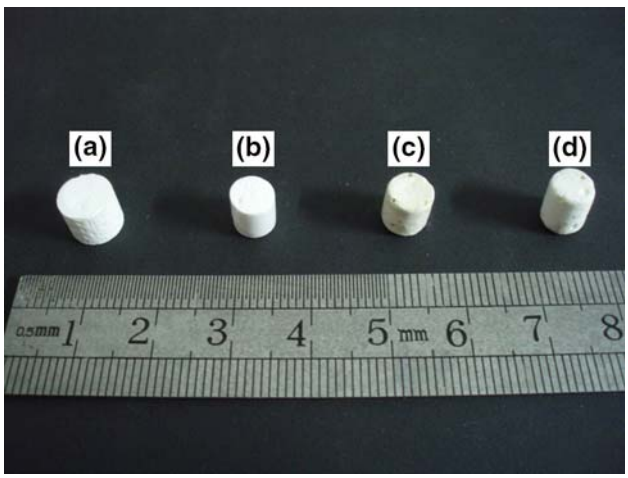

Fig. 3 Photographs of **a** PS template, **b** M-γ-Al_2O_3 support, **c** M–Pt/γ-Al_2O_3 and **d** M–K–Pt/γ-Al_2O_3

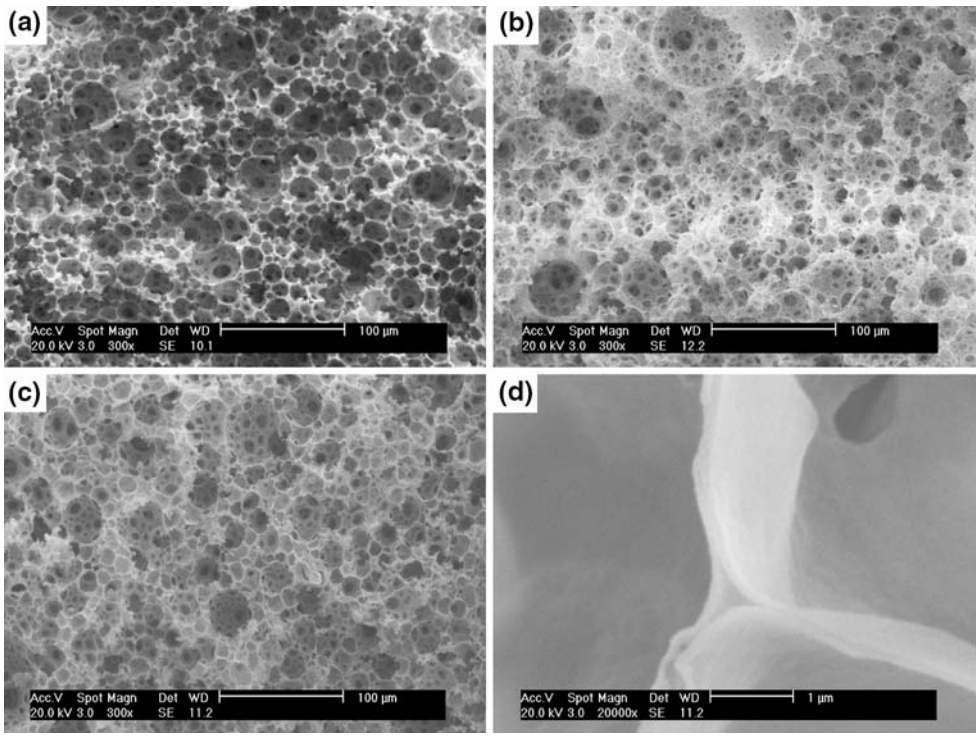

Fig. 4 SEM images of **a** PS template, **b** M-γ-Al_2O_3 support, **c** M–Pt/γ-Al_2O_3 and **d** high magnification of M-γ-Al_2O_3 support. Scale bar: 100 µm for (**a**, **b**, **c**) and 1µm for (**d**)

monolithic catalysts, as shown in Fig. 3c and d, take on a greyish colour which is due to the loading of platinum.

The SEM images of the template and the monolithic catalysts are shown in Fig. 4. Figure 4a is a representative picture of polystyrene foam monoliths, in which the macropores are in spherical shape and in diameter range of 10–50 µm. The spherical macropores are interconnected via windows with the diameters approximately 1–20 µm. The macropores were occupied by water during polymerization. After drying, the water vaporized, leaving interconnected macropores. The microscopic appearance of macro-porous alumina monolith (Fig. 4b) is the replica of the polystyrene foam with shrinkage taken into account. The walls of the alumina support consist of two layers of alumina located on both sides of the template walls, as can be seen from Fig. 4d. The wall thickness is about 0.3 µm. The Pt/Al_2O_3 and K–Pt/Al_2O_3 monolithic catalysts maintain the structure of the supports (Fig. 4c). The voidage of the alumina monoliths is about 0.80, which is close to the volume fraction of water added during preparing the polymer foam (0.82, see Sect. 2.1.1).

3.3 N_2 Adsorption–Desorption

Table 1 lists the BET surface areas and the average pore diameters of samples. The specific surface areas of macro-porous alumina monoliths and the Pt/Al_2O_3 monolithic catalysts are much larger than that of the particle alumina supports and the particle catalysts, respectively. For both of the monolithic catalysts and particle catalysts, loading of platinum led to a slight decrease of the specific surface area. As can be seen from Fig. 5, loading of platinum and potassium resulted in the pore volume (the amount of nitrogen adsorbed) of the monolithic catalysts decreasing and the pore diameter increasing (Table 1). This phenomenon should be due to blocking of the micropores of the support and/or sintering of the support in the impregnation and the following drying and calcination processes [26].

Table 1 BET surface area and pore diameter data of different samples

Sample	BET surface area (m^2 g^{-1})	Pore diameter[a] (nm)
P–γ-Al_2O_3	158	–
P–Pt/γ-Al_2O_3	141	–
M–γ-Al_2O_3	261	2.8
M–Pt/γ-Al_2O_3	235	3.8
M–K/Pt/γ-Al_2O_3	230	3.0

[a] BJH adsorption pore diameter

Figure 5 shows that the walls of the so prepared monolithic supports and monolithic catalysts contain meso and micro pores. Combined with the SEM images (Fig. 4), the macro-porous monolithic support and catalysts take on a multi-level porous structure, that is, the monoliths are enriched with interconnected macropores with meso and micro pores spreading over the walls of the macropores. In the words of Su et al. [27], the so prepared monolithic

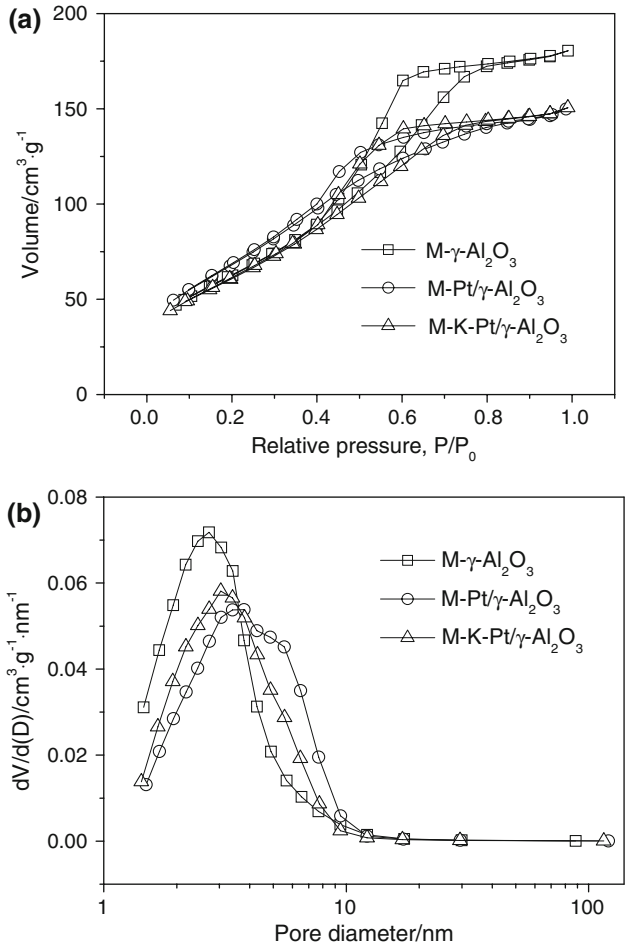

Fig. 5 N_2 adsorption–desorption and BJH pore size distribution curve of different catalysts. **a** N_2 adsorption–desorption curve, **b** BJH pore size distribution curve

supports and catalysts possess hierarchical macro-meso (micro)-porous structure, obviously which are much advantageous for reactants transferring and diffusing.

3.4 TEM

Figure 6 gives TEM pictures of the different catalysts. In P–Pt/γ-Al_2O_3 (Fig. 6a), Pt particles are uniformly and highly dispersed. The size of Pt is about 1.3 nm. As for M–Pt/γ-Al_2O_3 catalysts, the Pt particles are not homogeneously dispersed, some of Pt particles are in the size of about 1.6 nm (Fig. 6c), and some are in the size of about 10 nm (Fig. 6d). As point out by Nijhuis et al. [28], when drying a wet-impregnated monolith, the active component will move from the wetter parts of the monolith to the drier parts as a result of capillary forces. So the large Pt clusters should be formed during the microwave drying of the monolithic catalyst. In M–K–Pt/γ-Al_2O_3 catalysts, Pt particles size is about 3.3 nm and the Pt particles are homogeneously dispersed (Fig. 6b), which should be due to the modify effect of potassium. Potassium can prevent Pt clusters from aggregating and keep them highly dispersed [4, 6].

3.5 TPR

Figure 7 presents the TPR profiles of particle and monolithic catalysts. As shown in Fig. 7a and b, there are two reduction peaks for Pt/γ-Al_2O_3 catalysts. The reduction peaks between 200 and 300 °C are attributed to the reduction of PtO_x and/or PtO_xCl_y species on the support. The reduction peaks between 300 and 500 °C are assigned to the reduction of PtO_x and/or PtO_xCl_y species interacted with the alumina support [29]. The reduction peaks at 600–700 °C correspond to the reduction of potassium modified alumina, for the TPR profile of K/Al_2O_3 exhibits a similar peak at this temperature range.

The intensity of the peak at 200–300 °C in particle catalyst is obviously stronger than that in the monolithic catalyst, while the intensity of the peak at 300–500 °C in particle catalyst is weaker than that in the monolithic catalyst. This indicates that the interaction between platinum and alumina prefers to be formed in monolithic catalyst than in the particle catalyst, which should be due to the hierarchical pore structure. Adding potassium into the M–Pt/γ-Al_2O_3 catalyst led to the appearance of a sharp reduction peak at 220 °C, which attributes to the reduction of the surface oxygen provided by potassium [30]. On the other hand, adding of potassium resulted in an increase of the peak intensity at 200–300 °C and a decrease of the peak intensity at 300–500 °C, indicating that adding potassium is unfavorable for the interaction between platinum and alumina.

3.6 Catalytic Performance

As shown in Fig. 8a, CO conversions over P–Pt/γ-Al_2O_3 are higher than those over the crushed M–Pt/γ-Al_2O_3 catalyst in all reaction temperature range, indicating that the particle catalyst is more active intrinsically. Comparing the crushed and monolithic M–Pt/γ-Al_2O_3 catalyst, the CO conversions are much close to each other at the temperatures of $\leq$200 °C, while at the higher temperatures the difference is marked and the monolithic one gives higher CO conversion. Comparing P–Pt/γ-Al_2O_3 with M–Pt/γ-Al_2O_3 catalyst, CO conversions over the particle catalyst are higher as $\leq$200 °C, while the CO conversions over the monolithic catalyst are higher as >200 °C.

The difference between the crushed monolith and the monolithic catalyst is only that the monolith has macroporous structure while the crushed sample has not. The chemical structure and meso(micro) pore structure are the same for the crushed sample and the monolith. So the

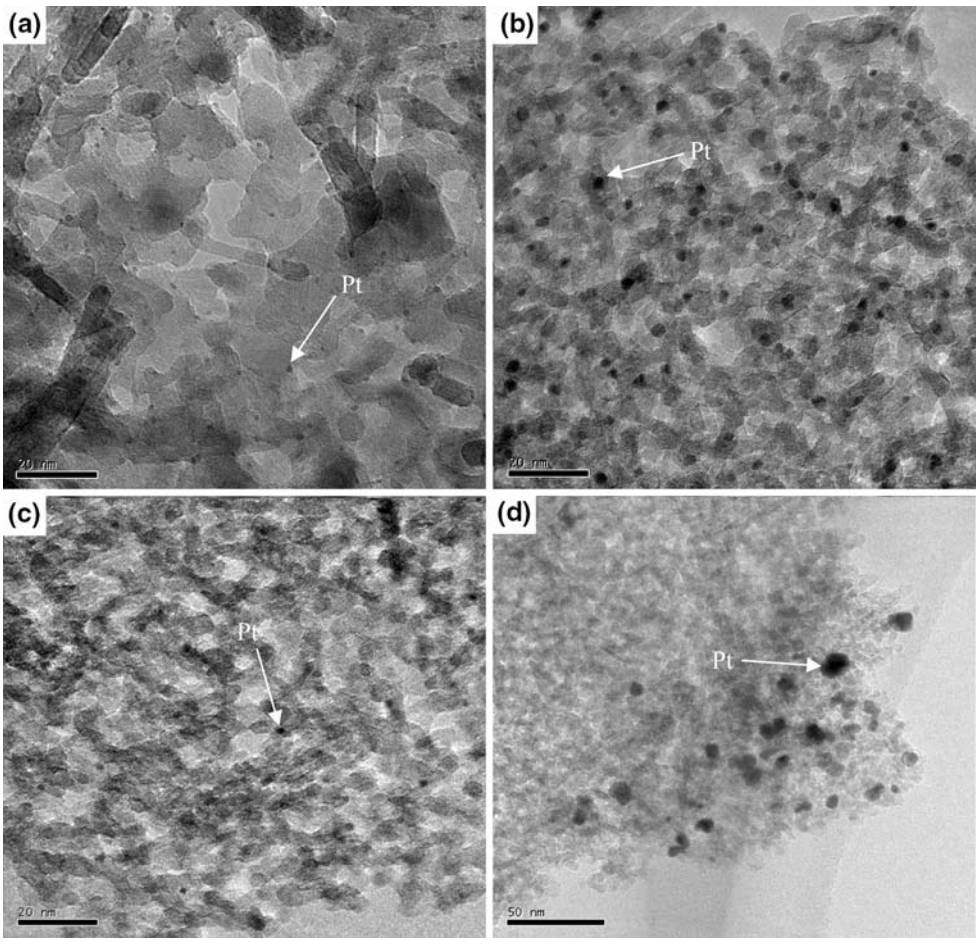

Fig. 6 TEM images of different catalysts after reduction **a** P–Pt/γ-Al_2O_3, **b** M–K–Pt/γ-Al_2O_3, **c**, **d** M–Pt/γ-Al_2O_3. Scale bar: 20 nm for (**a**, **b**, **c**) and 50 nm for (**d**). The arrowhead in each picture denotes a typical Pt particle

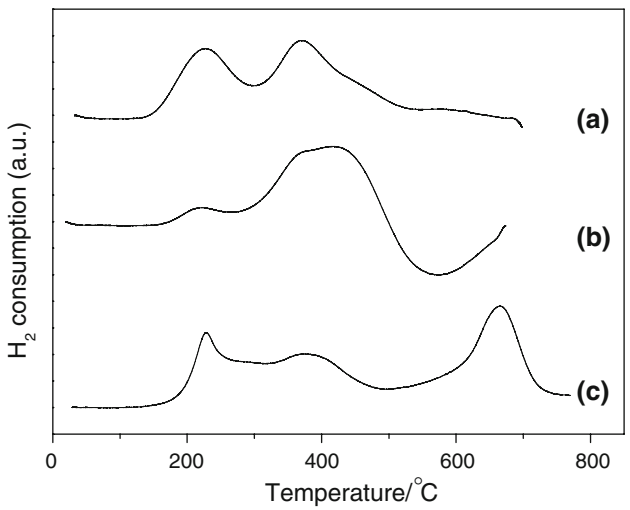

Fig. 7 TPR profiles of **a** P–Pt/γ-Al_2O_3, **b** M–Pt/γ-Al_2O_3 and **c** M–K–Pt/γ-Al_2O_3

intrinsic activity of the two should be the same. Hence, the higher CO conversion over the monolith is owing to the macro-porous of the monolith which favours mass transfer.

At the low temperatures, CO conversions are low, and the reaction rate should be determined by the surface reaction, representing mainly the intrinsic reactivity of the catalysts. At the high temperatures, CO conversions are high, and the reaction rate should be controlled by the diffusive resistance. So, the above results reveal that the intrinsic activity of particle catalyst is higher than that of the monolithic catalyst, but the CO removing efficiency is higher over monolithic catalyst (to note that CO-PROX process should be run at CO conversion close to 100%, that is, at the high temperatures). The highest CO conversion over the particle catalyst and crushed catalyst are only 91.2% and 72.9% exhibited at 225 °C. On the contrary, monolithic catalyst showed a lower intrinsic reactivity than the particle catalyst, but the porous structure of monolithic catalyst is good for mass and heat transfer, weakening the diffusive limitation. As a result, the CO removing efficiency is enhanced at higher temperatures. The highest CO conversion over monolithic Pt/γ-Al_2O_3 is 99.6% at 250 °C, corresponding to CO in exit gas of 40 ppm.

The intrinsic activity of the monolithic catalyst is lower than that of the particle catalyst should be due to the aggregation of the platinum particles as shown in TEM microscopy (Fig. 6d). The formation of methane over the monolithic catalyst also should be caused by the large

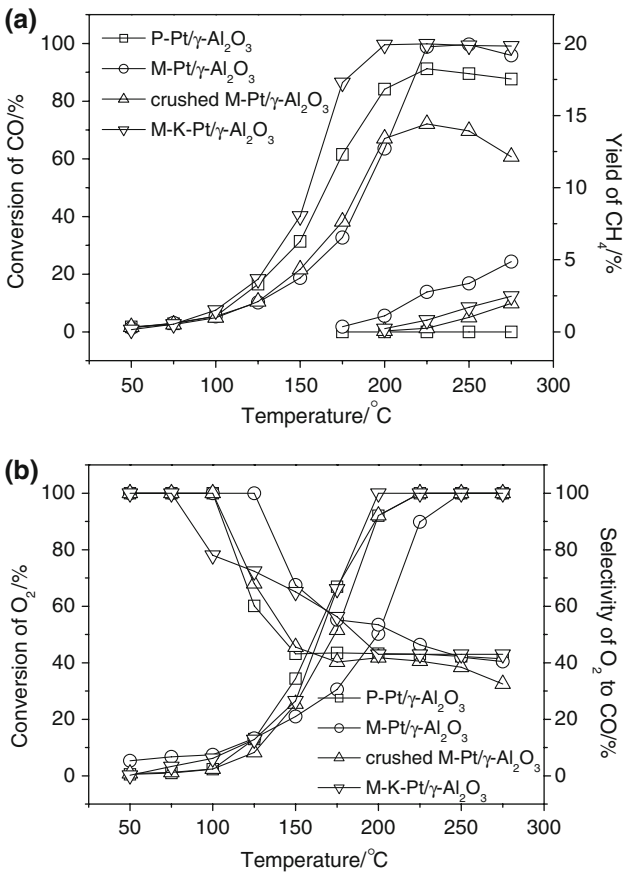

Fig. 8 Catalytic activity for CO-PROX over different catalysts. (**a**) Conversion of CO and yield of CH_4 vs. temperature, (**b**) Conversion of O_2 and selectivity of O_2 to CO vs. temperature. Reaction condition: 1 vol.% CO, 1 vol.% O_2, 50 vol.% H_2 in N_2, space velocity is 80,000 mL g_{cat}^{-1} h^{-1} (20,000 h^{-1})

platinum particles. In addition, TPR profiles (Fig. 7a, b) indicate that the amount of platinum interacted with alumina are more in monolithic catalyst than that in the particle catalyst, which is the other reason for the less activity of monolithic catalyst. It has been proposed that the high activity of Pt/Al_2O_3 catalysts is attributed mainly to the highly dispersed platinum corresponding to TPR peak at 200–300 °C and the formation of strong interaction between platinum and alumina is disadvantageous for the high activity [12].

From Fig. 8b, the O_2 selectivity to CO oxidation over the monolithic catalyst is higher than that over the particle catalyst. As mentioned in introduction section, CO oxidation is a diffusive controlled reaction, but H_2 oxidation is not. Macro-porous monolith is beneficial to mass transfer, which weakens the diffusive resistance and improves the conversion of CO oxidation. So, the monolithic catalyst improves the O_2 selectivity to CO oxidation.

Adding potassium into the M–Pt/γ-Al_2O_3 catalyst improves its catalytic activity and selectivity obviously (Fig. 8a). As reaction temperature is 200 °C or higher, the CO conversion over M–K–Pt/γ-Al_2O_3 catalyst is higher than 99%, and the yield of CH_4 is lower than the one without potassium. The highest CO conversion over M–K–Pt/γ-Al_2O_3 catalyst is 99.9%, corresponding to CO in exit gas of 10 ppm.

Kuriyama et al. [4–6] has proposed that the addition of potassium weakens the interaction between CO and Pt, which favors the conversion of CO to CO_2, thus improves its catalytic activity. TPR results of Fig. 7b and c show that adding potassium results in two variations: (1) more platinum species are in the state of highly dispersed nanoparticles and less platinum in strong interaction with alumina, (2) a new reduction peak appears which attributed to reduction of surface oxygen. The surface oxygen is in favor of CO oxidation. Both of them enhance the intrinsic activity of the monolithic catalyst. At the same time, the addition of potassium improved the platinum dispersancy (Fig. 5), which lead to the decrease of CH_4 formation (Fig. 8a).

On the other hand, micron/nanometer-monolithic catalytic reactor could be an important and a potential way for chemical process miniaturisation and process intensification. As for fuel cell oriented hydrogen production from hydrocarbons, miniaturisation is the key challenge [31]. For CO-PROX, a critical step for the hydrogen production, catalytic reactors such as honeycomb monolith (pore size in millimeter scale) and micro-reactor (channel width in several hundreds of microns) are widely studied for the miniaturisation [7, 8, 32–34]. As stated above, the pore size of macro-porous monolith is several tens of microns, which is much smaller than the channel size of honeycomb monolith as well as the channel width of the micro-reactor. So macro-porous monolith is probably a potential alternative for the miniaturisation.

Over honeycomb monolith catalysts, to remove CO to 10 ppm via CO-PROX, the volume space velocity is 7,000 h^{-1} as showed in our previous work [32, 33]. Over micro-channel reactor, the corresponding volume space velocity is 5,700 h^{-1} [34]. Over the macro-porous monolith of this work, the corresponding volume space velocity is 20,000 h^{-1} under the similar conditions. Higher volume space velocity means smaller volume of catalysts. Hence, the macro-porous monolith is a promising way for process miniaturisation, especially for fuel cell oriented hydrogen production from hydrocarbons.

4 Conclusive Remarks

For purifying CO in the hydrogen-rich stream by preferential CO oxidation to 10 ppm level, it needs not only to develop catalysts with high intrinsic activity, but also to optimize the porous structure of the catalysts. It is a

promising way to remove CO to ppm level by using macro-porous (the pore size is in micrometer or nanometer scale) monolithic catalysts or macro-meso(micro) -porous monolithic catalysts.

A very valuable indication of this work: for chemical process miniaturisation and process intensification, macro-porous monolith or macro-meso(micro)-porous monolith catalysts should be a potentially powerful alternative technique. Compared to honeycomb monolith and micro-channel catalytic reactor, the volume of macro-porous monolith should be much smaller.

In this work, macro-meso(micro)-porous monolithic catalysts of Pt/Al_2O_3 and K–Pt/Al_2O_3 were prepared, and the prepared monolithic catalysts present excellent effect for removing CO in hydrogen rich gases. Over the monolithic K–Pt/Al_2O_3catalyst, CO can be purified to less than 10 ppm at a space velocity of 80,000 mL g_{cat}^{-1} h^{-1} (20,000 h^{-1}) in reaction mixtures of 1 vol.% CO, 1 vol.% O_2, and 50 vol.% H_2 in N_2, indicating that macro-porous monolithic catalyst is a potential alternative for CO-PROX.

Acknowledgments The financial support of this work by Hi-tech Research and Development Program of China (863 program, Granted as No. 2006AA05Z115 and 2007AA05Z104) and the Cheung Kong Scholar Program for Innovative Teams of the Ministry of Education (No IRT0641) are gratefully acknowledged.

References

1. Ghenciu AF (2002) Curr Opin Solid State Mater Sci 6:389
2. Song C (2002) Catal Today 77:17
3. Trimm DL (2005) Appl Catal A Gen 296:1
4. Kuriyama M, Tanaka H, Ito S, Kubota T, Miyao T, Naito S, Tomishge K, Kunimori K (2007) J Catal 252:39
5. Tanaka H, Kuriyama M, Ishida Y, Ito S, Tomishige K, Kunimori K (2008) Appl Catal A Gen 343:117
6. Tanaka H, Kuriyama M, Shida Y, Ito S, Tomishige K, Kunimori K (2008) Appl Catal A Gen 343:125
7. Chin P, Sun X, Roberts GW, Spivey JJ (2006) Appl Catal A Gen 302:22
8. Roberts GW, Chin P, Sun X, Spivey JJ (2003) Appl Catal B Environ 46:601
9. Srinivas S, Dhingra A, Im H, Gulari E (2004) Appl Catal A Gen 274:285
10. Ayastuy JL, Gonzalez-Marcos MP, Gonzalez-Velasco JR, Gutiérrez-Ortiz MA (2007) Appl Catal B Environ 70:532
11. Ko EY, Park ED, Lee HC, Kim S (2007) Angew Chem Int Ed 46:734
12. Suh DJ, Kwak C, Kim JH, Kwin SM, Park TJ (2005) J Power Sources 142:70
13. Chang LH, Sasirekha N, Chen YW, Wang WJ (2006) Ind Eng Chem Res 45:4927
14. Avgouropoulos G, Papavasiliou J, Tabakova T, Iakiev V, Ioannides T (2006) Chem Eng J 124:41
15. Liu Y, Fu Q, Stephanopoulos MF (2005) Catal Today 93–95:241
16. Papavasiliou J, Avgouropoulos G, Ioannides T (2006) Appl Catal B Environ 66:168
17. Guo Q, Liu Y (2008) Appl Catal B Environ 82:19
18. Mariño F, Descorme C, Duprez D (2004) Appl Catal B Environ 54:59
19. Kolb G, Hessel V, Cominos V, Hofmann C, Löwe H, Nikolaidis G, Zapf R, Ziogas A, Delsman ER, de Croon MHJM, Schouten JC, de la Iglesia O, Mallada R, Santamaria J (2007) Catal Today 120:2
20. Ouyang X, Besser RS (2005) J Power Sources 141:39
21. Guliants VV, Carreon MA, Lin YS (2004) J Membrane Sci 235:53
22. Chen SL, Dong P, Xu K, Qi Y, Wang D (2007) Catal Today 125:143
23. Tan Q, Bao X, Song T, Fan Y, Shi G, Shen B, Liu C, Gao X (2007) J Catal 251:69
24. Somma F, Strukul G (2006) Catal Lett 107:73
25. Tokudome Y, Fujita K, Nakanishi K, Miura K, Hirao K (2007) Chem Mater 19:3393
26. Hwang CP, Ye CT (1996) J Mol Catal A Chem 112:295
27. Vantomme A, Léonard A, Yuan ZY, Su BL (2007) Colloids Surf A Physicochem Eng Aspects 300:70
28. Nijhuis TA, Beers AEW, Vergunst T, Hoek I, Kapteijin F, Moulijn JA (2001) Catal Rev 43:345
29. Yao HC, Sieg M, Plummer HK Jr (1979) J Catal 59:365
30. Lee CH, Chen YW (1997) Ind Eng Chem Res 36:1498
31. Kolb G, Hessel V (2004) Chem Eng J 98:1
32. Zeng SH, Liu Y, Wang YQ (2007) Catal Lett 117:119
33. Zeng SH, Liu Y (2008) Appl Surf Sci 254:4879
34. Kin KY, Han J, Nam SW, Kim TH, Lee HI (2008) Catal Today 131:431